Chapter 1 - Introduction

1.1 History

Metallic glasses have some amazing properties that captured my imagination and determined my path for grad school. In APh 110, Winter term 2003-2004, Dr. William L. Johnson gave a seminar lecture describing his research with an enthusiasm that was intoxicating. He described amorphous metals, materials having a random arrangement of atoms that were frozen in a liquid configuration because of a clever choice of alloying elements. These elements were chosen to have large negative heats of mixing and near eutectic compositions meaning the elements were much happier mixed than separate. The atomic sizes of alloying elements were also chosen so that many different sized spheres can log jam efforts of the mixture to crystallize upon cooling from the molten state.

Dr. Johnson's most famous alloy is a ZrTiCuNiBe composition called Vitreloy 1. This alloy was so resistant to crystallization that 1 inch thick samples could be cooled amorphous. The material conducted electricity like a metal, had strength in tension and hardness as high as the best steels with elastic limits ten times greater than crystalline metals. It could be die cast like aluminum because the melting temperature of the alloy was half that of steel and it had an interesting softening behavior at the glass transition temperature that opened possibilities of processing the material like a plastic.

To recap: There is a material as strong and hard as cutting edge steels with the ability to be formed like a plastic. This is something I had to study!

The metamorphosis of this theoretical possibility, plastically processing a metallic glass, into reality, provided endless hours in my laboratory playground pursuing interesting avenues of research that made for a wonderful grad school experience.

1.2 Physics of Metallic Glasses

Below the glass transition temperature, metallic glasses are liquids stuck in one configuration. They are formed by rapidly quenching molten material. As the material cools, a competition between thermodynamics and kinetics ensues. Thermodynamics requires that materials exist in the lowest energy state at a given temperature. Below the melting temperature, the lowest energy state for materials is a crystal. To form a crystal however, the atoms must move into a crystalline configuration. As a liquid cools, the viscosity of the liquid increases or stated another way, the mobility of the atoms decreases. If a material can be cooled quickly enough to limit atom mobility and frustrate crystallization, a glass is formed. The speed at which an alloy must be cooled to frustrate crystallization is called its glass forming ability (GFA). Due to the slower cooling rate of thicker samples, another measure of GFA is an alloy's critical casting thickness. Critical casting thickness is the maximum diameter a cylindrical sample can be cast amorphous (see Derivation 1).

A glass at room temperature can be reheated above T_g to a viscous liquid state where the mobility of the atoms increases as a function of temperature. This increased mobility allows the glass, which bypassed crystallization when originally cooled from the melt, to sample various configurations and eventually the crystalline state is found. Most heating processes are too slow to bypass crystallization of metallic glasses, but one alloy very resistant to crystallization, PdNiCuP, has been cooled from the molten state to room temperature and then reheated to the molten state with no crystallization [1].

These thermodynamic properties can be measured in a Differential Scanning Calorimeter (DSC). The amount of heat required to equalize the temperatures of an

empty reference crucible and a crucible with a known weight of sample is measured as a function of temperature. The heat difference divided by the mass of the sample is the heat capacity of the sample. A plot of the heat capacity as a function of temperature for a typical metallic glass (MG) is a good starting point to discuss the thermodynamics of these materials. Figure 1.1 shows a typical DSC scan for a MG. The glass transition temperature, T_g, the crystallization temperature, T_x, the solidus temperature, T_s, and the liquidus temperature, T_L, are shown along with the enthalpy of crystallization, H_x, the enthalpy of fusion, H_f and the magnitude of the discontinuity in heat capacity Δc_p.

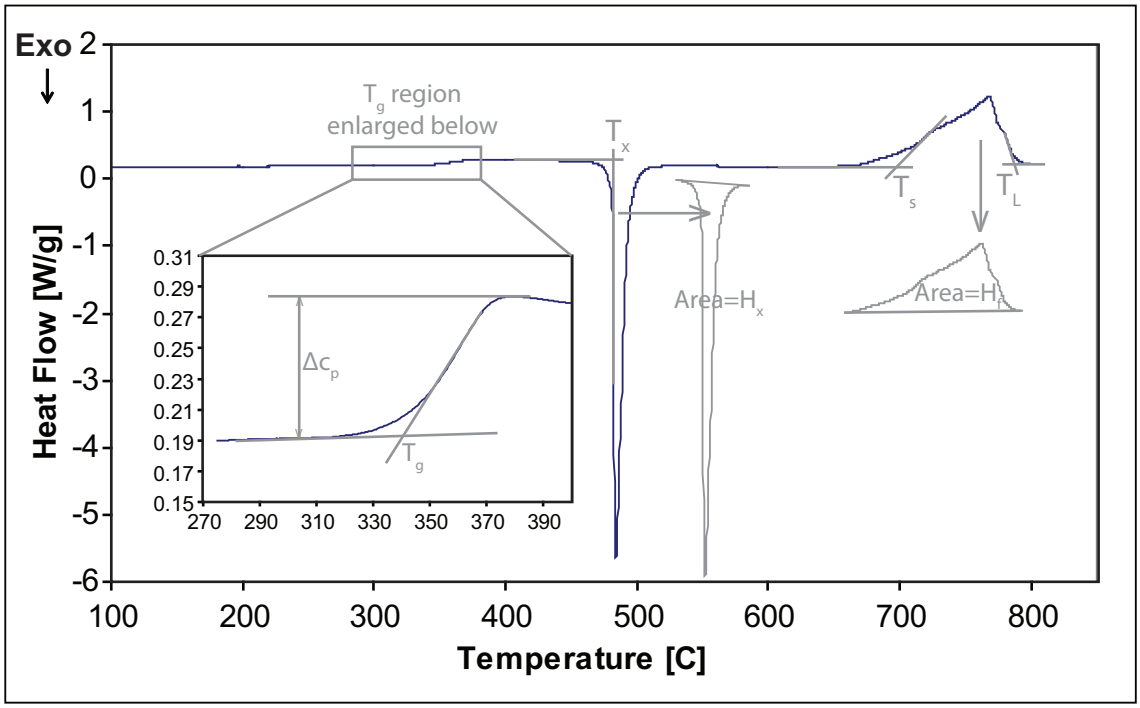

Figure 1.1: DSC scan of $Zr_{44}Ti_{11}Cu_{20}Be_{25}$ showing heat capacity features characteristic of metallic glasses. Inset region on left shows glass transition region and maintains axis units of large plot.

These variables need further explanation. The glassy sample begins at room temperature and is heated above its glass transition temperature. The physics of the glass transition is still being debated. Some claim that it is a second order phase transition [2]

and that glasses are a unique phase of matter. The less controversial explanation follows the kinetics argument above and defines T_g as the temperature at which the material begins to flow. The glass transition is visible as a discontinuous jump in heat capacity = Δc_p. In the kinetics argument, Δc_p arises from changes in the slope of the volume, entropy, and enthalpy curves at the glass transition due to the kinetic freezing of the liquid [2] (see Derivation 2). Above T_g, the mobility of the atoms in the undercooled liquid increases and at T_x a crystalline configuration is found and the sample reaches the desired thermodynamic low energy crystalline state. As the sample transitions from a high energy liquid to a low energy crystal, heat must be released and the exothermic crystallization peak is observed. The total heat released in the crystallization process is H_x. The temperatures at which melting begins and ends are T_s and T_L respectively. In an elemental solid, melting peaks are very sharp and theoretically $T_s = T_L$. Melting a solid is an endothermic process meaning that heat input is required to cause the phase change from crystal to liquid. The amount of heat required to melt the crystal = H_f. If the sample was heated quickly enough, crystallization and melting would not have occurred and the glass could be taken back above the crystalline melting temperature with only a discontinuity in heat capacity.

The ability of a metallic glass to resist crystallization at temperatures above T_g is called its thermal stability. This is of course a time and temperature dependant parameter. The longer a MG is left at a temperature above T_g, the more configurations the atoms can explore and eventually the sample will crystallize. Additionally, the atoms move more quickly and explore configurations more quickly at higher temperatures. Both T_g and T_x as measured in a DSC will depend on heating rate. Exact values for T_g

and T_x are impossible to obtain because they are tied to the kinetics of the atoms. In much of the scientific literature on MG and for most of this thesis, thermodynamic data is collected at heating rates of 20 K/min. The value $T_x - T_g = \Delta T$ is one measure of the thermal stability of a MG. ΔT is also called the width of the supercooled liquid region (SCLR), so named because the material has regained flow properties of a liquid, but exists at "super cooled" temperatures well below the melting temperature.

Another quantitative measure of the thermal stability of an alloy is summarized in a time temperature transformation (TTT) diagram. TTT diagrams depict the results of rapidly bringing a MG to a given temperature and then measuring the time to the onset of crystallization at that temperature. Asymmetries exist in TTT diagrams constructed by cooling molten material and waiting for crystallization vs ones constructed by heating glassy material and waiting for crystallization [3]. The authors of [3] discuss the asymmetry in terms of classical nucleation theory and suggest that crystal nuclei are formed upon cooling and then grow at different rates upon heating above T_g. Heating and cooling TTT diagrams for the Zr based alloy with the highest known GFA, $Zr_{41.2}Ti_{13.8}Cu_{12.5}Ni_{10}Be_{22.5}$ [3-5], are presented in Figure 1.2. Notice the rounded shape of the cooling TTT curve. The shortest time is marked T_n on the temperature axis indicating the "nose temperature." At this temperature, the thermodynamic driving force to crystallize and mobility of the atoms combine to be optimal for crystallizing in the shortest possible time. At temperatures higher than T_n, the mobility of atoms is greater, but there is less thermodynamic driving force to crystallize. At temperatures lower than T_n, the thermodynamic driving force is higher, but the mobility of the atoms is too low. These concepts are shown in Figure 1.3.

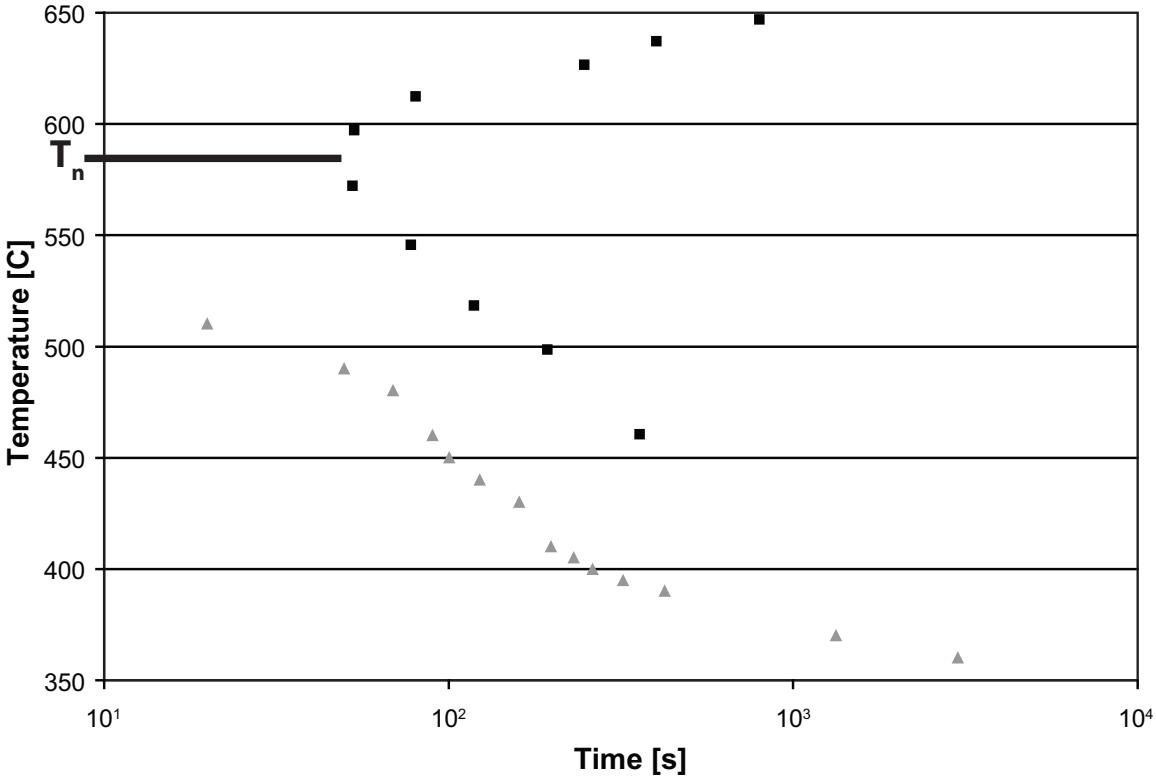

Figure 1.2: TTT diagram upon heating (▲) and cooling (■) for $Zr_{41.2}Ti_{13.8}Cu_{12.5}Ni_{10}Be_{22.5}$.

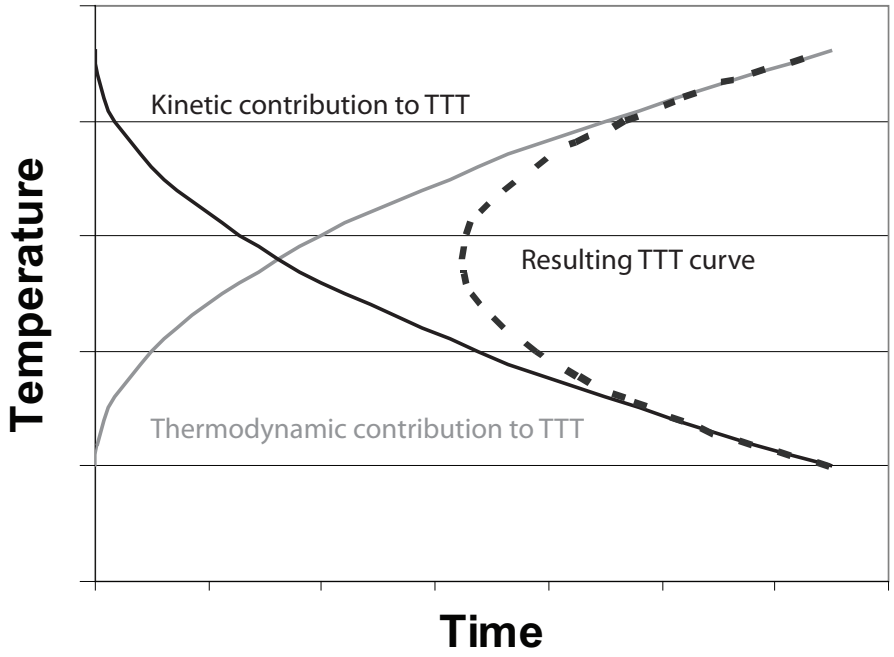

Figure 1.3: Schematic TTT plot shown with high mobility (kinetics) and low driving force (thermodynamics) at high temperature and low atom mobility with high thermodynamic driving force at low temperature creating a nose in the TTT curve at intermediate temperatures. The thermodynamic driving force would go to zero (infinite time) above the liquidus temperature.

We know that a MG begins to flow at T_g and stops flowing at T_x (liquid to solid transition) upon heating. Flow can be thought of in terms of shear stresses, i.e., how does one layer of material move with respect to another as they slide across each other. The fundamental equation governing viscosity is $\frac{dv}{dr} = \frac{F}{\eta}$ where F is the applied shear stress, η is the viscosity, and *dv/dr* is the spatial derivative of the velocity orthogonal to the shear direction. This equation can be solved for many testing geometries. The parallel plate geometry is solved in Derivation 3. Measurements of viscosity as a function of temperature are also possible and a good mathematical fit to η(T) data is achieved using the Vogel-Fulcher-Tammann (VFT) equation presented in Derivation 4 [6].

The physics of MG flow has been a subject of much interest in the MG community [7]. Johnson et al. examined flow of MG from a microscopic perspective. Given that MG are multicomponent alloys, there should be a smallest length scale at which the properties of the glass are observable. In crystals, this length scale is the unit cell and a periodic arrangement of unit cells recreates the crystal and its properties. In MG a "unit cell" is most closely approximated by a shear transformation zone, STZ. Experiments suggest that STZ may be as small as 200 atoms [7]. One can not periodically arrange STZ because they approximate fundamental units of an amorphous material and are not space filling. There are compatibility stresses required to place STZ in space. As the name suggests, an STZ will shear given an appropriate temperature and stress and accommodate movement in the SCLR. Analysis of flow assuming a distribution of STZ sizes and energy wells each STZ sits in is contained in Derivation 5.

The result is an equation with less fitting parameters than the VFT equation that better fits η(T) data of MG. The equation is:

$$\frac{\eta}{\eta_\infty} = Exp\left[A\left(\frac{T_g}{T} \right)^{m/A} \right]$$

Where η is the temperature dependant viscosity, η_∞ is the high temperature viscosity or can be approximated by the plank limit viscosity ~ 10^{-5} Pa-s, A = Log(η_g/η_∞) where η_g = 10^{12} Pa-s, and m = Angell fragility.

The Angell fragility is defined as follows:

$$m = \frac{\partial Log(\eta)}{\partial (T_g / T)}$$

The Angell fragility gives the slope of the Log(η(T_g/T)) curve. This is a valuable parameter because it determines how steep the η(T) plot will be. Fragile liquids or materials with high m soften quickly above their glass transition temperature and exhibit steeper η(T) relationships.

The physics of the SCLR in some alloys is even more complicated than we have discussed so far. Phase separation in metallic glasses has been claimed in many glass forming alloy systems including AuPbSb [8-9], ZrCu [10], ZrTiBe [11-14], ZrTiCuNiBe [15-17], MgCuYLi [18], CuZrAlAg [19], TiYAlCo and ZrYAlCo [20]. X-ray scattering has shown splitting of the broad amorphous spectrum in as-cast AuPbSb glass [8]. Additionally Small Angle Neutron Scattering (SANS), Small Angle X-ray Scattering (SAXS), Anomalous Small Angle X-ray Scattering (ASAXS), observation with Transmission Electron Microscopy (TEM), rheology measurement anomalies, resistivity measurement anomalies, and Differential Scanning Calorimetry (DSC) measurements showing apparent double glass transitions are some of the techniques used to support the

claims of phase separation. Some AuPbSb and ZrTiBe glasses are thought to have two glasses in as-quenched samples. Other alloy systems are thought to phase separate upon annealing.

Much of the work on phase separation in the Vitreloy (ZrTiNiCuBe) system is relevant to this thesis. Johnson and collaborators conducted SANS experiments on Vitreloy compositions after various annealing times and temperatures [15-17]. As-cast samples exhibited only background scattering, but after annealing, the maximum scattering intensity was peaked about $q = 0.5\ A^{-1}$ and indicated a quasiperiodic arrangement of scattering inhomogeneities. SAXS and ASAXS experiments determined that the annealing led to the segregation of the alloy into Zr rich and Ti rich amorphous phases. This composition variation was found to happen at a length scale of about 13nm. After this amorphous phase separation, the crystallization pathway becomes quite complex. Kelton found a stable icosahedral phase in the TiZrNi phase diagram from ab initio calculations [21]. Evidence of the icosahedral phase has been found in various Vitreloy compositions by indexing X-ray diffraction patterns of alloys crystallized by isothermal annealing in the SCLR [22-24]. TEM observation of quasicrystal phases has also been accomplished [23-24]. The SANS peak is seen to shift as a function of annealing temperature as predicted by the Cahn-Hilliard theory for spinodal decomposition. Annealing at temperatures higher than the amorphous phase decomposition region causes spinodal decomposition of the alloy into nanocrystalline regions [15-17]. Some postulate that the quasicrystals phase precipitates from the phase separated glass and later provides the nucleation site for other crystal phases [22-24]. Slight coarsening of the nanocrystals has been observed with annealing, but the length

scale only increased to about 40nm [17]. Other compositions in the same Vitreloy alloy family did not phase separate into amorphous phases upon annealing [16]. Johnson and collaborators proposed a miscibility gap and a spinodal decomposition region in the SCLR of the ZrTiNiCuBe phase diagram and proposed rough composition boundaries.

Tanner and Ray examined the ZrTiBe system for glass forming compositions and found many alloys could be made amorphous in 100μm thick ribbons [11-14]. Heat capacity measurements conducted in a DSC on some of the compositions revealed two discontinuities in heat capacity in the supercooled liquid region (SCLR). A glassy material is expected to exhibit one discontinuity in heat capacity at the glass transition temperature as the material transitions from solid-like to liquid-like behavior and becomes able to flow [2]. Two jumps in heat capacity, and an apparent double glass transition temperature are unusual. Tanner proposed that this anomalous feature in the heat capacity was due to the presence of two glassy phases.

There are some in the metallic glass community who dispute the existence of the two phases in many of these systems and attempt to explain the data in alternative ways [25-28]. Perhaps the most controversial alloy thought to show two phases is $Zr_{36}Ti_{24}Be_{40}$. Hono showed that TEM work done by Tanner supporting the existence of two phases in the $Zr_{36}Ti_{24}Be_{40}$ alloy was flawed and proved that the observed "phases" were in fact etching artifacts [27]. The apparent double glass transition has been suggested to be a single glass transition with a neighboring exothermic ordering event prior to crystallization [26]. This explanation could be plausible given the evidence of quasi crystal formation in the more complicated Vitreloy system, especially in light of TEM work showing what appear to be ordered phases after deformation of the in the

SCLR of the $Zr_{36}Ti_{24}Be_{40}$ alloy [25]. Discussion and experiments supporting the two phase glass argument in the ZrTiBe system will be discussed further in Chapter 6.

1.3 Applied Physics (for processing) in Metallic Glasses

Armed with the concepts of viscosity, thermal stability and TTT diagrams we can consider what properties a metallic glass must posses to be a good candidate for processing like a plastic in the SCLR. The plastic forming process we sought to replicate was injection molding. A simple injection molding process requires feedstock material, a heated reservoir in which the material is softened, a nozzle, a mold and a plunger to force the softened material from the reservoir through the nozzle into the mold. Typical plastic injection molding occurs at temperatures of 180 - 340 °C and viscosities of 10^2 - 10^3 Pa-s. Time is a minimal constraint because polymers and plastics typically have enormous thermal stabilities due to the long tangled molecular chains that kinetically resist organization into a crystalline structure. 60 - 300 s is a reasonable time to thermally equilibrate the feedstock material and inject it into the mold.

A metallic glass must have good enough GFA to make macroscopic specimens to be a viable candidate for feedstock material. The metallic glass community calls an alloy a bulk metallic glass (BMG) if the GFA is high enough to allow 1mm diameter rods to be cast fully amorphous. BMG forming alloys also have the advantage of having better thermal stability on cooling as compared to alloys with poorer GFA.

Processing a BMG using a method similar to injection molding in the SCLR however, requires high thermal stability of the glass upon heating. In order to look at the relevant parameters for processing in the SCLR we invented a new kind of plot for metallic glasses. Because temperature is the easiest parameter to vary in the injection

molding process, we combined the TTT data upon heating with η(T) data for an alloy of interest eliminating the temperature variable. This created an ηTT or viscosity time transformation plot. An ηTT plot is shown in Figure 1.4 for the well known $Zr_{41.2}Ti_{13.8}Cu_{12.5}Ni_{10}Be_{22.5}$, Vitreloy 1, composition. TTT and η(T) data is only tabulated for a few alloys in the literature because the measurements are very time consuming. Therefore another parameter is needed to compare the majority of BMG forming alloys.

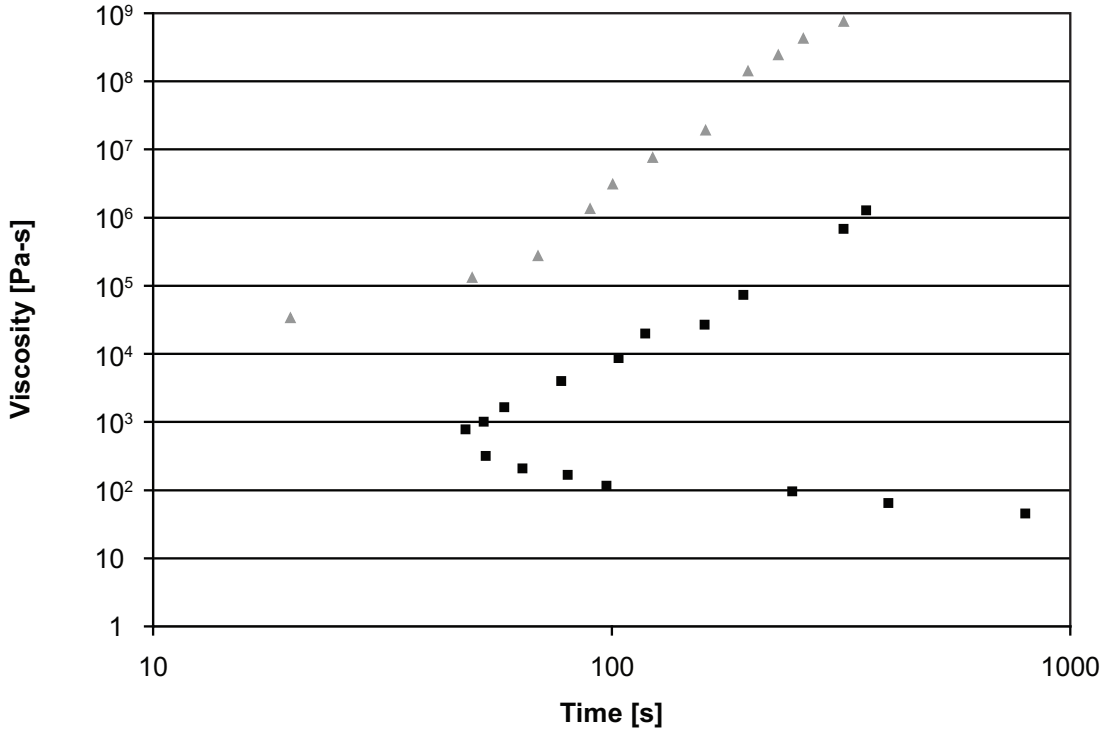

Figure 1.4: ηTT plot for $Zr_{41.2}Ti_{13.8}Cu_{12.5}Ni_{10}Be_{22.5}$ using heating TTT data (▲) and cooling TTT data (■). This plot looks upside down compared to Figure 1.2 because lower viscosities occur at higher temperatures.

If an oversimplification is made and all BMG are assumed to have similar fragilities, then the dominant term predicting the lowest available processing viscosity in the η(T) equation derived by Johnson et al. [7] is $T_x - T_g = \Delta T$. ΔT is also a measure of an alloy's thermal stability upon heating. Measurement of ΔT for a BMG forming alloy

takes less than one hour and ΔT data is tabulated for many compositions. This could be a simple way of eliminating many compositions from consideration as potential alloys for plastic forming processes in the SCLR.

Another method to measure formability of glassy alloys in the SCLR was suggested by Schroers [29]. Schroers proposed that $0.1cm^3$ of material could be compressed between parallel plates under a specified load at a constant heating rate through the SCLR until crystallization of the glassy material stopped the flow. A schematic diagram illustrating this test is presented in Figure 1.5 (modified from Chapter 4). The diameter of the squished disk would be a measure of the formability with larger diameters indicating higher formability in the SCLR. This method closely resembles viscosity determination in a parallel plate rheometer, but explores the entire SCLR in one measurement. For alloys with known fragility, a parameter to predict formability can be derived from the Johnson η(T) equation [7] coupled with the ideas behind the squish test method proposed by Schroers. The basic idea is to integrate the area between the infinite temperature viscosity line and the η(T) equation over the SCLR. The parameter is presented in Derivation 6.

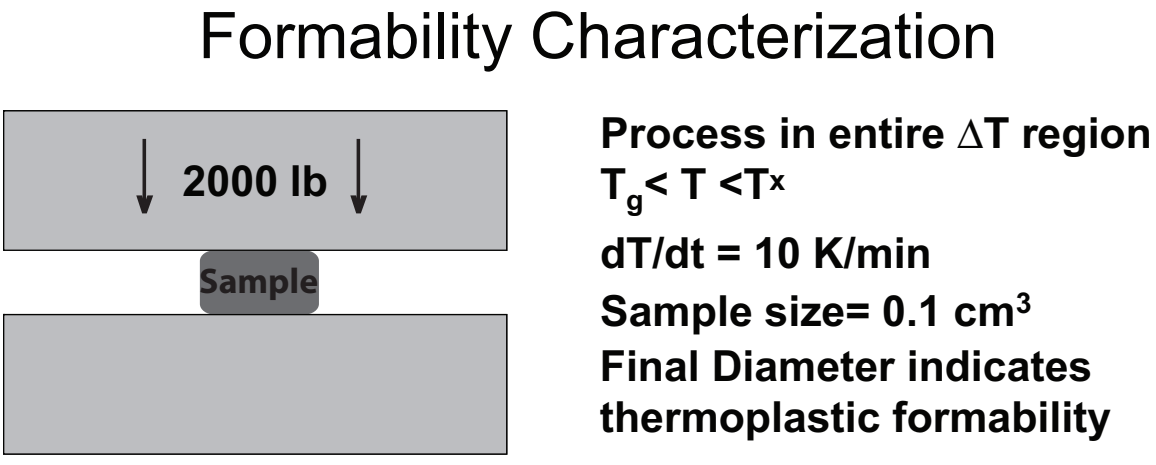

Figure 1.5: Schematic of squish test proposed by Schroers.

1.4 Advantages of Thermoplastic Processing and State of the Field in 2005

Most practical applications of MG demand near net-shaping process in manufacturing. The most common method of obtaining metallic glass parts is die casting wherein molten alloy is injected into a mold and then cooled below the glass transition temperature sufficiently fast to avoid crystallization. Die casting requires the molten alloy to be quickly introduced into the mold and then rapidly quenched before the onset of crystallization. This processing route takes advantage of the thermodynamic stability of the alloy at temperatures above the crystallization nose, T_n in the TTT diagram showed in Figure 1.2. At the temperature T_n, an alloy has the minimum time to crystallization. Porosity is introduced into the sample due to the high inertial forces in relation to the surface tension forces realized during the injection of the molten liquid, which gives rise to a Rayleigh-Taylor instability and consequent flow breakup resulting in void entrapment. Porosity is also found in the center of die cast parts because parts are cooled through contact with a mold from the outside in and cavities nucleate in the center due to large negative pressures present in the center of parts cooled in this manner. The cooling requirements of die casting bound the dimensions of die cast parts to no larger than can be cooled sufficiently fast to avoid crystallization and no smaller than can be quickly filled. Parts with complex geometries, thin sections, and high aspect ratios are difficult to obtain with die casting.

The unique advantages of injection molding, blow molding, micro replication, and other thermoplastic technologies are largely responsible for the widespread uses of plastics such as polyethylene, polyurethane, PVC, etc., in a broad range of engineering applications. Powder Injection Molding (PIM) of metals represents an effort to apply

similar processing to metals, but requires blending of the powder with a plastic binder to achieve net shape forming and subsequent sintering of the powder. Given suitable materials, thermoplastic forming (TPF) would be the method of choice for manufacturing of metallic glass components because TPF decouples the forming and cooling steps by processing glassy material at temperatures above T_g and below T_x followed by cooling to ambient temperature [30-31]. To clear up some terminology difficulties it should be noted that forming in the SCLR, thermoplastic forming, and plastic processing all refer to the same process of applying pressure to deform an alloy heated to a temperature in the SCLR. A polymer or plastic material made up of long carbon chains also exhibits a T_g and is processed in this manner, thus the terminology "plastic" processing.

Thermoplastic forming methods take advantage of the kinetic stability of an alloy at temperatures below the crystallization nose. TPF decouples the fast cooling and forming of MG parts inherent in die casting and allows for the replication of small features and thin sections of metals with high aspect ratios. TPF methods also take advantage of lower processing temperatures resulting in relatively lower oxidation rates. TPF has several advantages over conventional die casting, including smaller solidification shrinkage, less porosity of the final product, more flexibility on possible product sizes, and a robust process that does not sacrifice the mechanical properties of the material. TPF methods include the forming of amorphous metal sheets [32], the compaction of amorphous powders [33], the extrusion of amorphous feedstock into a die [34], and the imprinting of amorphous metal [35]. Most of these routes reduce the porosity of the processed amorphous part but have limitations. Forming of amorphous metal sheets limits the thickness of the final sample and the available part geometries.

Powder compaction methods usually produce parts having micro or nano dispersed porosity which often results in inferior mechanical properties compared to homogenously solidifying parts. Free extrusion, or extrusion into a die only allows parts with simple geometries to be fabricated. Imprinting methods enable very small features to be replicated, but are incapable of producing bulk parts. Figure 1.6 gives a pictorial summary of some of the parts created with thermoplastic forming techniques. It is easily seen in Figure 1.6 that fabrication of the depicted parts required relatively small strains. In fact, all the parts formed using TPF methods prior to the work described in Chapter 5 of this thesis were limited to small strains.

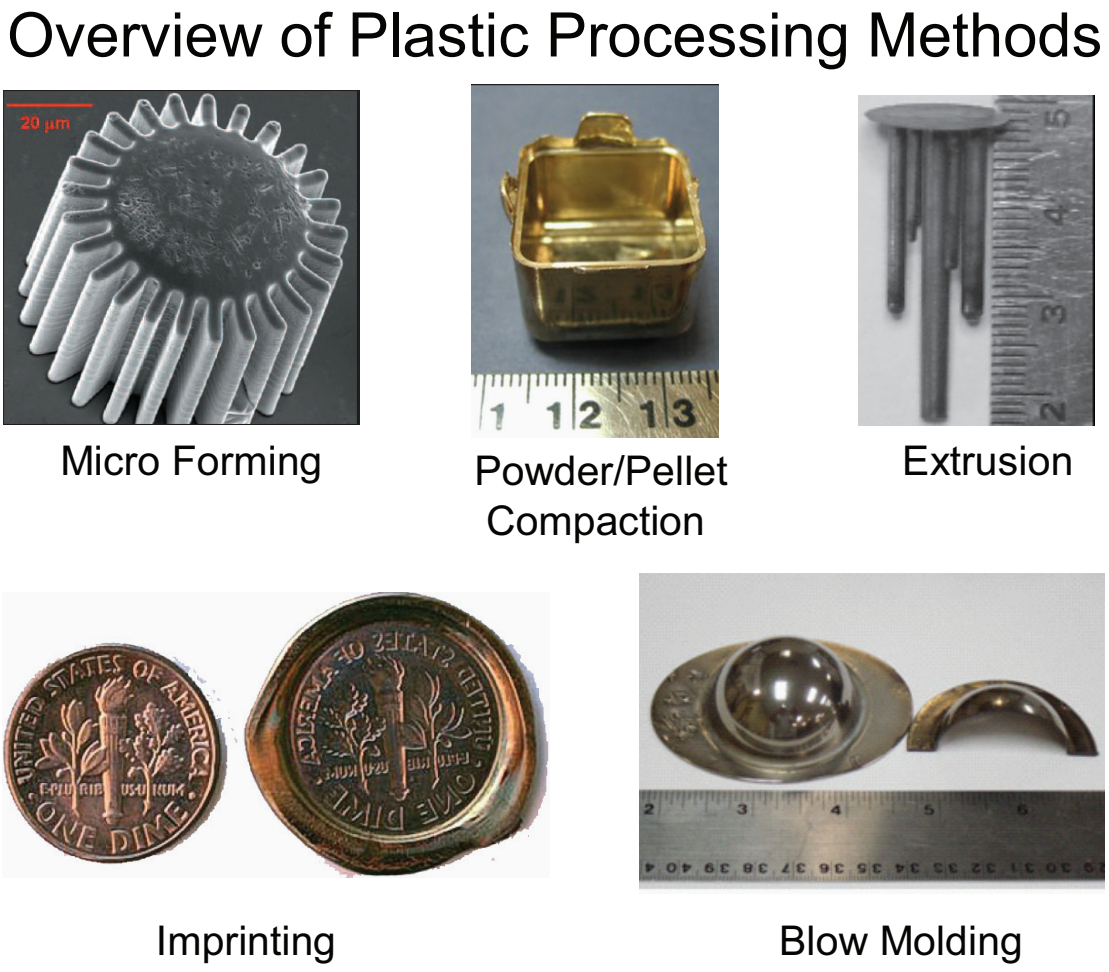

Figure 1.6: Thermoplastic forming demonstrations 2005-2007 [30-31, 36-37].

The goal of injection molding is to use the ability of metallic glasses to flow homogeneously at temperatures between T_g and T_x to enable pressurized injection of the alloy into a mold to produce a homogenous bulk part with no size restrictions. This method would require higher strains than previously achieved by any of the thermoplastic forming methods prior to 2005.

A perfect BMG forming alloy that could be swapped for polymer plastics in injection molding and similar plastic forming processes would have the following properties:

- Thermal stability in the SCLR for 60 - 300 s
- A viscosity of 10^2 - 10^3 Pa-s
- A processing temperature of 180 - 340 °C

In 2005 when my graduate studies began, there were hundreds of BMG forming compositions to choose from. Metallic glass forming alloy compositions are given in atomic percent unless otherwise stated and the family to which a particular alloy belongs is determined by the element with the highest atomic percentage. Some of the families we considered were Au, Pd, Pt, Zr, Ti, Ce, Y, La, Mg, Ca, Co, and Fe based alloys [38-39]. Y, La, Co, and Fe based alloys are known for low fracture toughness and are therefore mechanically undesirable. Ce, Ca, and Mg based glasses are often prone to corrosion. Au based alloys have very high fragility but often the T_g is near room temperature and the alloys crystallize readily. Zr, Ti, Pd, and Pt based BMG were examined for suitability to forming processes in the SCLR.

A literature search revealed many attempts at forming in the SCLR prior to 2005. Some of the best results to date are presented in Figure 1.6. The favored alloys were

$Pd_{43}Ni_{10}Cu_{27}P_{20}$, $Pt_{57.5}Ni_{5.3}Cu_{14.7}P_{22.5}$, $Zr_{41.2}Ti_{13.8}Cu_{12.5}Ni_{10}Be_{22.5}$ (Vitreloy 1), and $Zr_{44}Ti_{11}Cu_{10}Ni_{10}Be_{25}$ (Vitreloy 1b). TTT diagrams and η(T) measurements had been published prior to 2005 for many of these alloys and DSC data existed for all of them. The alloys all had large ΔT values ranging from the smallest value for $\Delta T_{Vit\ 1} = 65$ °C to $\Delta T_{Vit\ 1b} = 135$ °C. The Pd and Pt based glasses have smaller ΔT values, but higher fragilities making all these alloys good candidates for TPF. In the last four years, publications from other research groups, and work within the Johnson group has fleshed out the data necessary to construct ηTT plots for all these compositions. Figure 1.7 contains heating and cooling ηTT plots for the good TPF candidate alloys. It is quickly seen that the alloys are limited to viscosities greater than 10^5 Pa-s for the processing times required for injection molding and similar TPF processes using the ηTT plots for heating. Only a cooling ηTT plot for $Pd_{43}Ni_{10}Cu_{27}P_{20}$ is presented. There are multiple conflicting sets of data for heating the Pd alloy. The Pd alloy differs from other alloys because Pd based alloys are able to be fluxed and cleaned with B_2O_3. Fluxing Pd based alloys with B_2O_3 under inert gases allows the alloys greater thermal stability and resistance to crystallization. Fluxed and unfluxed samples have very different TTT plots because unfluxed alloys crystallize at much shorter times for a given temperature than their fluxed counterparts. In an injection molding process conducted in air, the unfluxed behavior is what would be observed. The Pd based alloy shows the most promise for TPF of the alloys examined so far, but falls short of what would be needed to replace a plastic.

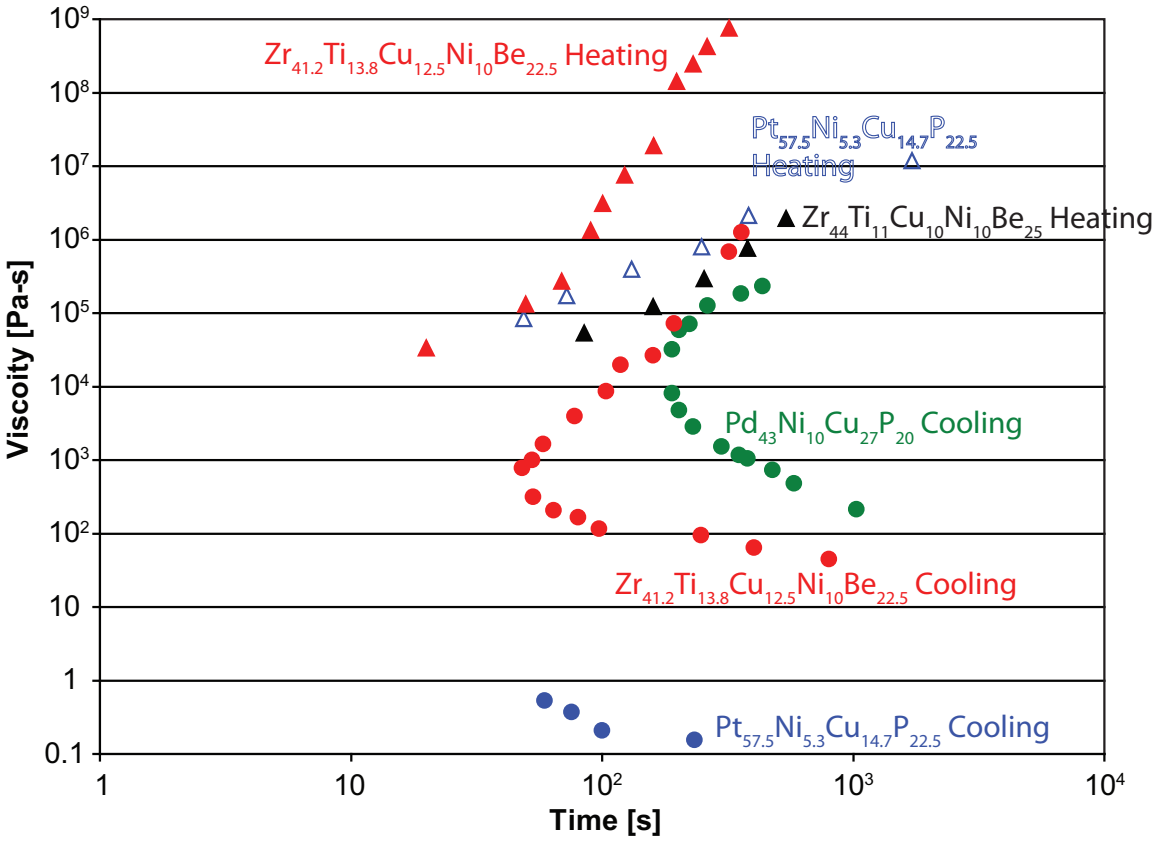

Figure 1.7: ηTT plots for alloys commonly used in TPF processes. GFA for the Pt alloy is insufficient to obtain the entire cooling TTT curve. No cooling TTT data is available for $Zr_{44}Ti_{11}Cu_{10}Ni_{10}Be_{25}$. Conflicting heating TTT data for the Pd alloy is not presented. Data taken from [1, 5, 7, 40-41].

From a processing point of view, BMG alloys with an extremely large supercooled liquid region (excellent thermal stability against crystallization), which can provide lower processing viscosities and exhibit smaller flow stress, would be desirable for use in conjunction with a TPF process. In addition, excellent GFA and low glass transition temperature (T_g) are also preferred properties for MG used in TPF processes. Unfortunately, among the published metallic glasses, no suitable alloys existed [42-44]. Zr based metallic glasses, especially the Vitreloy series, are much less expensive than Pt and Pd based alloys, have exceptional glass forming ability, but they have low fragilities and low processing viscosities are unattainable in the SCLR [45-48].

Accordingly, a need exists for a new family of inexpensive MG that can be incorporated into a thermoplastic processing application.

1.5 Alloy Development Strategies

The value of ΔT was the easiest parameter to measure and seemed to give a good indication of TPF potential so we set out to find alloys with larger ΔT values. Without a strategy, success in alloy development can be as likely as winning the lottery. Approaching the problem scientifically and not just rolling the dice was the key. Even then, it took a few iterations before finding the right method.

The first strategy to find alloys with larger ΔT values that met with limited success was based on the phase separation work discussed in Section 1.2 in the ZrTiCuNiBe, Vitreloy, system. Given that some of the Vitreloy compositions showed phase separation upon annealing in the SCLR which led to formation of a quasicrystal phase and eventual nanocrystallization, it was thought that we could increase ΔT by suppressing the quasicrystalline phase. Kelton's work predicted a stable TiZrNi quasicrystal [21]. The simplest solution to suppress a TiZrNi phase is to remove all Ni from the alloys.

The alloy with the largest ΔT found by this method was the all Cu version of Vitreloy 1b, $Zr_{44}Ti_{11}Cu_{20}Be_{25}$. Unfortunately, $\Delta T_{vit\ 1b\ all\ Cu} = 135$ °C. We hadn't lost anything in ΔT by removing all the Ni, but also hadn't gained anything.

Exploring quinary composition space in the Vitreloy system is very cumbersome. Assuming we coarse grained the system into 5% composition steps, we would need to create 10626 alloys to tile the composition space. The combinatorics for 1 - 5 component alloys is included in Derivation 7. It takes approximately 2 hours per alloy to weigh,

melt, cast and run a DSC scan. This task could be accomplished in just over 10 years of 40 hour work weeks. If we explored a ternary composition space, we would only need 231 alloys to tile the system. Tanner explored the ZrTiBe system in the 1970s [11-14] and found that compositions with 30 – 60% Be could be made amorphous in thin foils. Additional work by Tanner using the CALPHAD method to predict ternary phase diagrams from binary phase diagram data found the region of composition space expected to have the lowest melting temperature alloys [49]. This near eutectic region occupied a triangle with 30 - 45% Be. Using this prior work by Tanner and the ternary phase space simplification, we were able to significantly diminish the number of alloys necessary to explore the composition space. The ternary alloy development is detailed in Chapter 3 of this thesis.

The next alloy development strategy challenged many of the assumptions about GFA in the Vitreloy family held in the BMG community in 2005. It was assumed because of the work by Tanner that alloys in the ZrTiBe system were limited in GFA to thin foils 10 - 100μm thick [11-14, 50-51]. Thanks to Dr. Peker's work and patent it was also assumed that the GFA of Vitreloy type alloys was only attainable by adding late transition metals (LTM) from the columns containing Mn, Fe, Co, Ni, or Cu on the periodic table [4, 52]. Both these assumptions turned out to be false. In order to stay outside the Peker patent, only alloys free of LTM were tested. ZrTiBe compositions with GFA high enough to cast 1 - 6mm diameter rods were found. This means that the critical cooling rates required to create amorphous ZrTiBe samples were 100 - 1000 times lower than previously thought. Additions of V, Nb, and Cr were found to raise the GFA of alloys to as high as 8mm diameter casting thickness. Bulk glass forming alloys with

densities as low as crystalline Titanium were discovered having compressive yield strengths as high as Vitreloy compositions [53-54]. Some of the highest strength to weight ratio metals in existence are among these alloys. The low density and no LTM alloy development details and hallmark alloys are more thoroughly discussed in Chapter 2 of this thesis. The alloy with largest ΔT value discovered using this strategy of alloy development, $Zr_{35}Ti_{30}Be_{35}$, only had $\Delta T = 120$ °C.

It became clear that our last option was to venture back into Peker patent territory by adding LTM to the ternary compositions. It is important to have a mental picture of what each alloying addition accomplishes to know what direction to move for further improvement. For instance the alloy $Zr_{35}Ti_{30}Be_{30}Cu_5$ could be thought of as

- 5% Cu substitution of Zr in $Zr_{40}Ti_{30}Be_{30}$
- 5% Cu substitution of Ti in $Zr_{35}Ti_{35}Be_{30}$
- 5% Cu substitution of Be in $Zr_{35}Ti_{30}Be_{35}$

The property we sought to maximize was ΔT. Adding a LTM to the alloys had the added bonus of increasing GFA. DSC plots of the ternary alloys and quaternary alloy which could be thought of as Cu substitution for the various elements are included in Figure 1.8. Figure 1.8 suggests that LTM substitution should be thought of as a fourth element being substituted for Be in order to maximize ΔT.

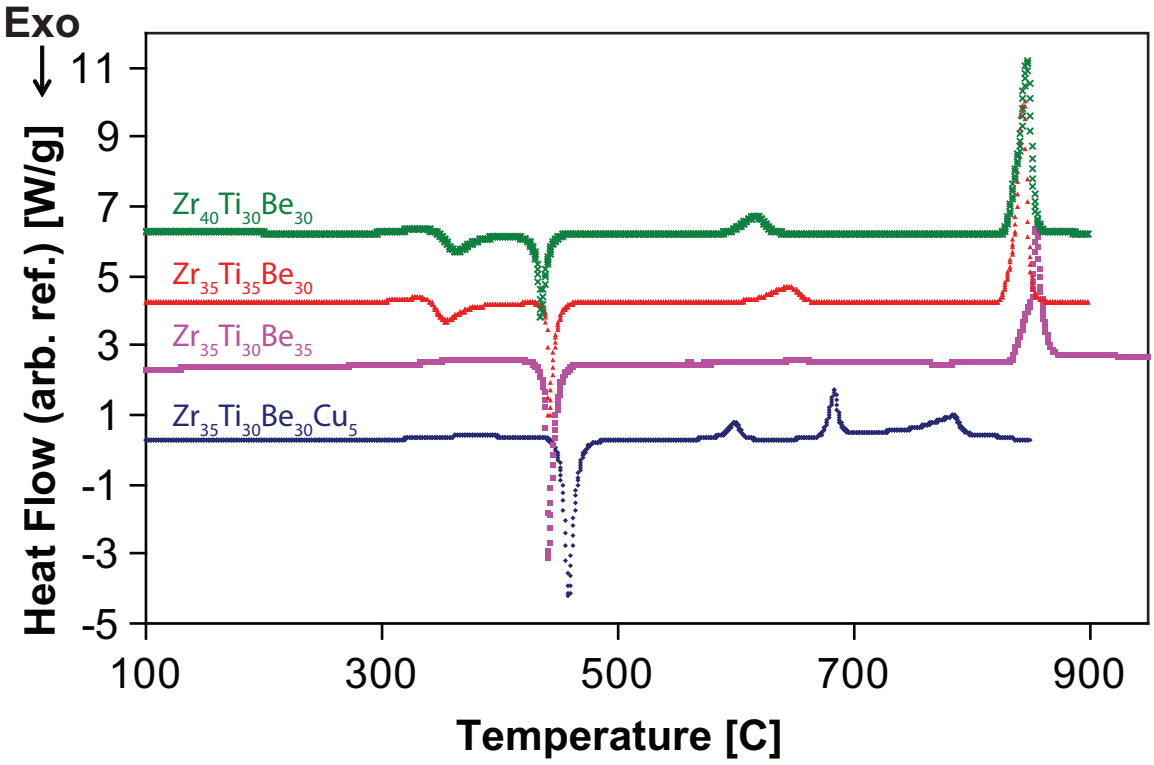

Figure 1.8: Quaternary alloy with 5% Cu plotted at bottom of figure. This quaternary alloy could be thought of as 5% substitution of Cu for Zr, Ti, or Be in the ternary alloys going top down. $Zr_{35}Ti_{30}Be_{35}$ has a SCLR most similar to the quaternary alloy so Cu substitution for Be is the most useful way to think of these alloys to maximize ΔT.

We identified the ternary compositions with the largest ΔT and replaced Be with increasing amounts of LTM until ΔT stopped increasing. This strategy was extremely successful. We tried Co, Fe, Ni, and Cu substitution for Be and found Cu to be the best alloying addition. We found 12 alloys with ΔT larger than 150 °C and three alloys with ΔT larger than 160 °C. An alloy based on the ternary composition with the largest ΔT turned out to be the optimal alloy for our purposes. $Zr_{35}Ti_{30}Be_{27.5}Cu_{7.5}$ had ΔT = 165 °C. Our work in alloy development increased the thermal stability of Vitreloy type glasses by over 20% and opened up possibilities for injection molding a metal. The addition of LTM to create quaternary alloys with the largest known ΔT values of any metallic glass is detailed in Chapter 3 of this thesis.

1.6 What To Do with All These Alloys

Grad students often daydream about being one of those scientists so accomplished they get equations or physical constants or even elements named after them. Einstein, Curie, Fermi, Nobel, Mendel, Bohr, Lawrence, Rutherford, Meitner, and Seaborg all made it to the Periodic Table of the Elements. Some of us in the Johnson group wished to play a hand in our scientific immortality and decided to name alloys after ourselves. Elements have the suffix "ium" added after the name and in order to differentiate our alloys from elements, we had to come up with a new suffix. Indisputably Amorphous Metal, "IAM," seemed like a good suffix that would sound elemental. It further amused because of the biblical reference in Exodus, and because the plural, IAMS, could be confused for a dog food. Just to make sure these alloys are in print and not limited to oral histories of the Johnson research group they are recorded here.

- Aaroniam $Zr_{35}Ti_{30}Be_{29}Co_6$
- Marioniams A class of Ni and Cu free Pd glasses [55]
- O'Reillyam / O'Reilliam $Zr_{35}Ti_{30}Be_{30}Al_5$*

*In honor of my favorite news commentator, I have named a cutting edge alloy after Bill O'Reilly. This alloy, O'Reillyam (O'Reilliam) is less dense than others in its family and can withstand a corrosive environment 1,000,000 times longer than its precious-metal sister.

After inventing and naming the alloys, some of the properties needed to be studied. The squish test proposed by Schroers, as a way to rank thermoplastic formability of different alloys, was performed on the alloys favored for TPF in the literature, namely, $Pd_{43}Ni_{10}Cu_{27}P_{20}$, $Pt_{57.5}Ni_{5.3}Cu_{14.7}P_{22.5}$, $Zr_{41.2}Ti_{13.8}Cu_{12.5}Ni_{10}Be_{22.5}$ (Vitreloy 1), and

$Zr_{44}Ti_{11}Cu_{10}Ni_{10}Be_{25}$ (Vitreloy 1b) as well as the alloy we invented with the largest ΔT, $Zr_{35}Ti_{30}Be_{27.5}Cu_{7.5}$. The squish test indicated that $Zr_{35}Ti_{30}Be_{27.5}Cu_{7.5}$ had the best potential for TPF of any of the alloys tested. Details of the squish test are included in Chapter 4 of this thesis.

$\eta(T)$ and TTT measurements for $Zr_{35}Ti_{30}Be_{27.5}Cu_{7.5}$ were taken to quantitatively determine the TPF. Details of these experiments in Chapter 4 reveal a surprisingly high fragility was calculated for this alloy that does not fit well with other Vitreloy alloy data. It has been neglected so far, but many of the ternary alloys showed the double discontinuity in heat capacity that Tanner proposed was evidence of two glasses. Many of the quaternary compositions based on the "two T_g" ternaries also showed the double jump in heat capacity. A more detailed study of the flow properties of these materials with the two T_g events is included in Chapter 6 of this thesis. The unusual flow properties of these materials may be the reason for the high fragility calculated for $Zr_{35}Ti_{30}Be_{27.5}Cu_{7.5}$ which exhibits the two T_g phenomenon. A plot in Chapter 5 of ηTT (using heating data) for the commonly used TPF alloys and the newly invented $Zr_{35}Ti_{30}Be_{27.5}Cu_{7.5}$ verify as the squish tests did that $Zr_{35}Ti_{30}Be_{27.5}Cu_{7.5}$ is the best available for TPF applications like injection molding. That plot is reprinted here as Figure 1.9.

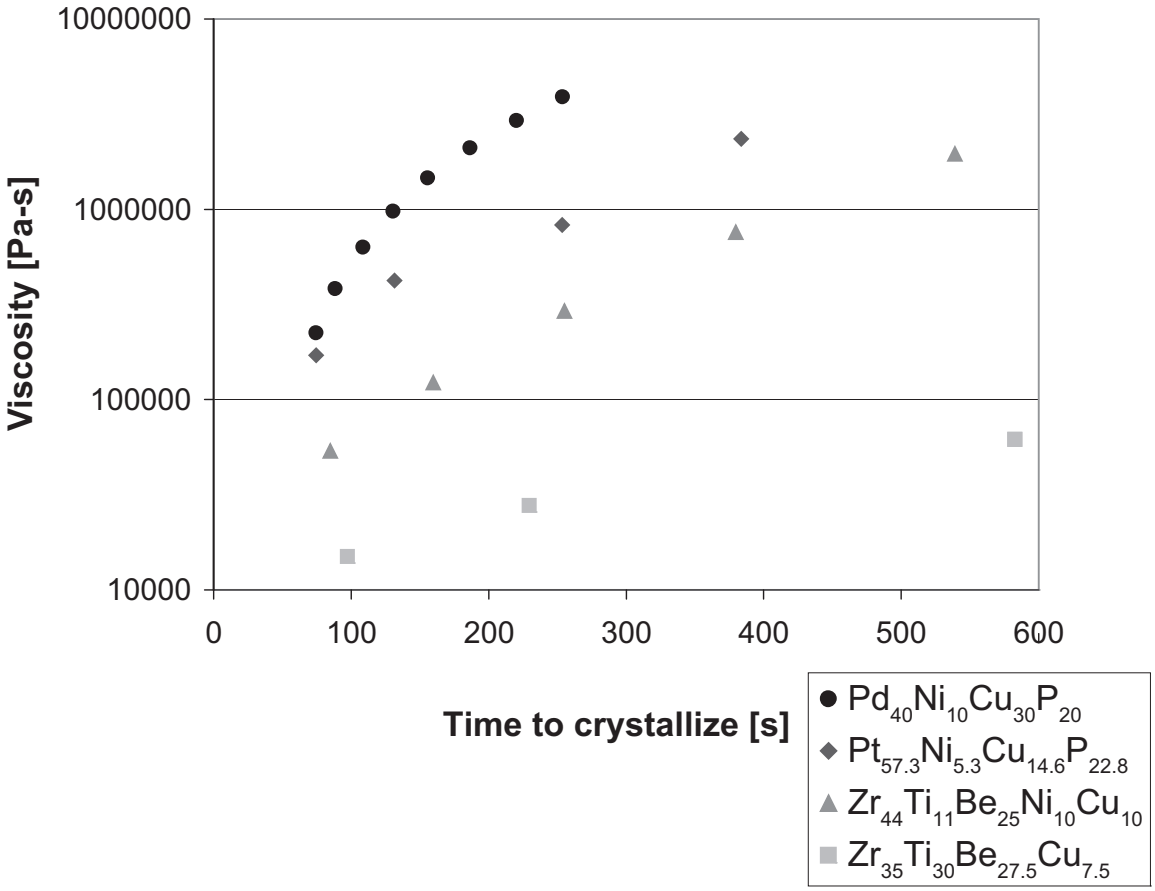

Figure 1.9: Time to crystallization versus viscosity plot for four thermoplastically processable alloys. This plot combines TTT and viscosity versus time data to show available processing time for a given viscosity for the alloys [7, 37, 40-41, 56]. Figure reproduced in Chapter 5.

A TPF process like injection molding takes 60 - 300 s. If we look at Figure 1.9, we see that $Zr_{35}Ti_{30}Be_{27.5}Cu_{7.5}$ has 10 times lower processing viscosities in that time frame than any other metallic glass. This is a huge alloy development success, but unfortunately not a candidate to replace plastics in injection molding because plastics process at 10^2 - 10^3 Pa-s while this alloy only reaches viscosities of 10^4 Pa-s at the times required for injection molding.

Determined to have some success after this much work, we modified an injection molding setup to maximize the nozzle diameter, increase the available force, and heat the feedstock to temperatures higher than those used for processing plastics. As we tried to

make $Zr_{35}Ti_{30}Be_{27.5}Cu_{7.5}$ feedstock we ran into additional problems. Alloys are melted on an arc melter and if the ingot cools amorphous, the value of $\Delta T \sim 165$ °C. If the alloy is remelted and cast into a mold, ΔT decreases. We tried various temperatures and hold times while melting the alloy in quartz tubes and water quenching and the value of ΔT decreased. The details of this study are included in Chapter 5.

Finally we decided that amorphous ingots from the arc melter must be used as feedstock material. The bottom of the ingots however had a thin crystalline layer because of direct contact with the cooled hearth and had to be cut off with a diamond saw. After verifying that the ingots were completely amorphous, multiple attempts at injection molding were made using varying temperatures and pressures. The modifications were successful and the first ever injection molded metallic glass part was created. A figure showing the polished injection molded part from Chapter 5 is included below as Figure 1.10. The injection molded part had superior mechanical properties to a die cast specimen of the same dimensions. Details can be found in Chapter 5.

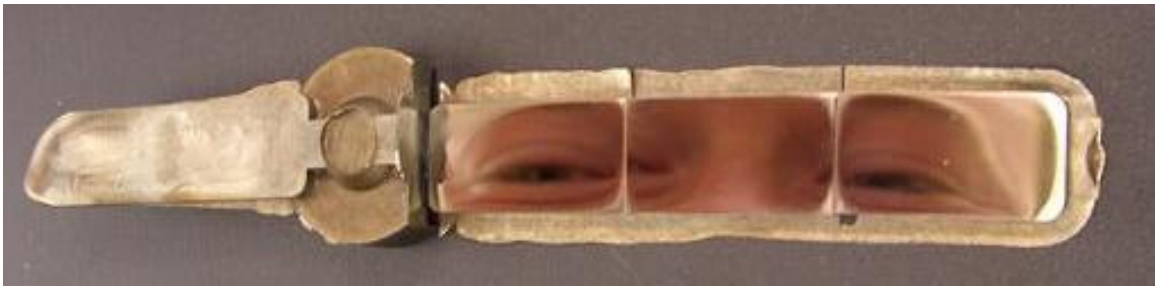

Figure 1.10: Photograph of the polished injection molded part prior to final sectioning for three-point bend testing.

Viscosity measurements performed on $Zr_{35}Ti_{30}Be_{27.5}Cu_{7.5}$ had some unusual characteristics that were neglected in the push to be the first person to injection mold a metallic glass. A DSC scan of the SCLR of $Zr_{35}Ti_{30}Be_{27.5}Cu_{7.5}$ is magnified to show the

apparent two T_g phenomenon in Figure 1.11. Viscosity measurements of this alloy would show small deformation for the first 50 °C after the calorimetric T_{g1} and then the deformation rate would increase dramatically after the calorimetric T_{g2}. After successfully injection molding this alloy, curiosity prompted a revisiting of the ternary alloys that showed the most prominent discontinuities in heat capacity.

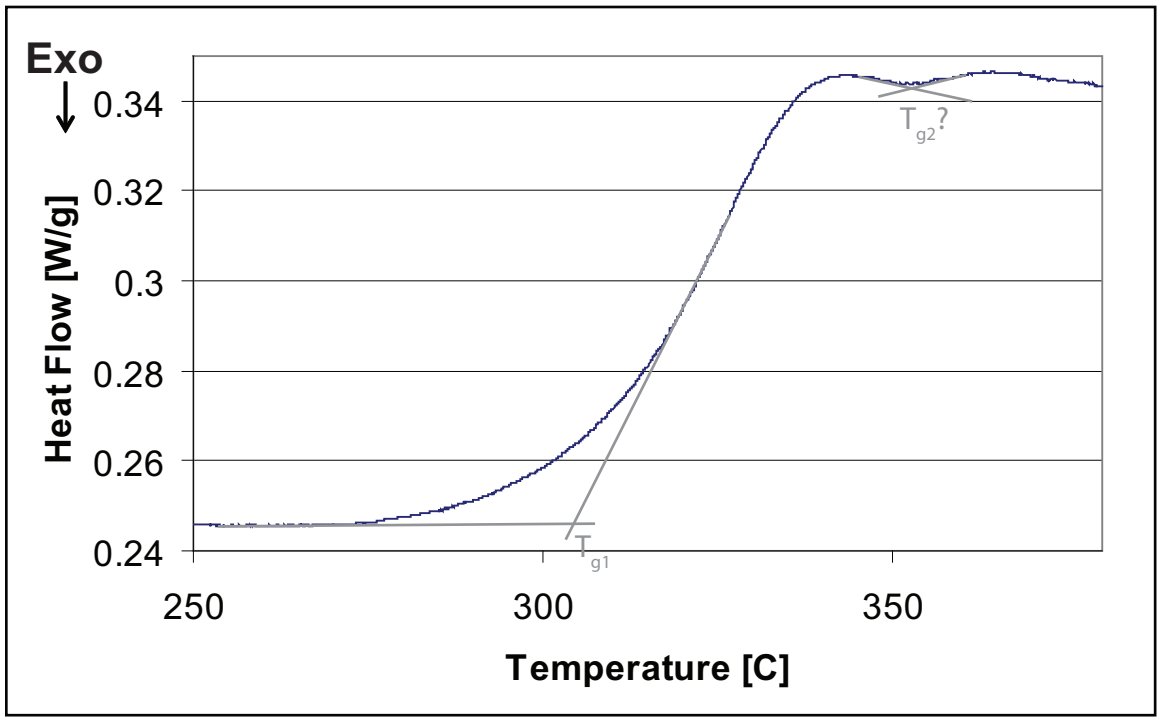

Figure 1.11: Apparent two T_g phenomenon seen in 20 K/min DSC scan of $Zr_{35}Ti_{30}Be_{27.5}Cu_{7.5}$.

The ternary alloys with the most prominent double heat capacity discontinuities lay along the $(Zr_aTi_{1-a})_{60}Be_{40}$ composition line. Three regions of flow were observed in these alloys with discontinuities in the slope of the η(T) measurements roughly correlating to the T_g values measured in the DSC. Figure 1.12 shows a representative viscosity curve superimposed with a DSC curve for this composition line. The alloy should have about 60% of the low T_g phase and 40% of the high T_g phase. Viscosity is plotted on the left vertical axis, temperature is along the x axis and the heat capacity is

along the right vertical axis. Although there is some controversy in the BMG community over the existence of two phases in these alloys, the flow behavior can be nicely explained with the two phase assumption. In region 1, both phases are below their glass transition temperatures and would behave like solids. In region 2, the phase with the lower T_g softens and the other phase is still below its T_g so a solid + liquid flow is observed. In region 3, the second glass softens at temperatures above T_{g2} and we get liquid + liquid flow, where the two liquids have different viscosities. A large body of theoretical work has been done on two phase flow and with some hefty assumptions, a qualitative picture of what a two phase glass $\eta(T)$ plot should look like is included in Derivation 8. The analysis predicts changes of slope in $\eta(T)$ as observed experimentally.

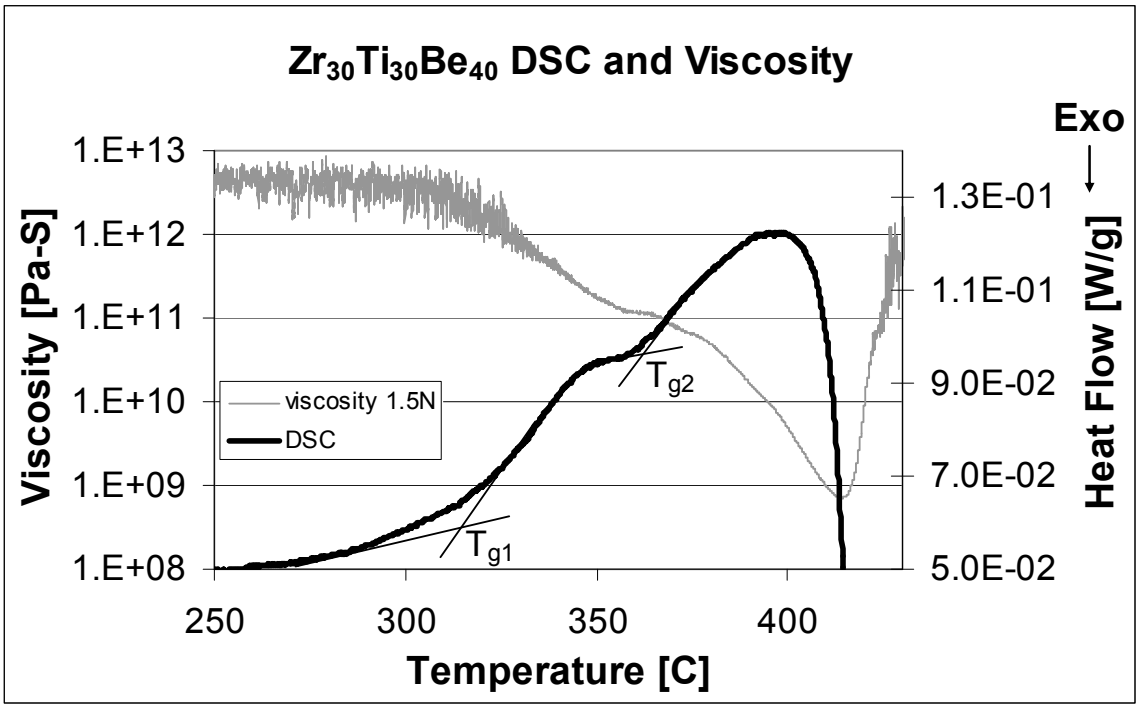

Figure 1.12: DSC and viscosity curve plotted against temperature for $Zr_{30}Ti_{30}Be_{40}$ which shows about 60% of the low T_g phase and 40% of the high T_g phase. The viscosity plot shows two flow regions roughly corresponding to the discontinuities in heat capacity seen in the DSC.

If we assume that the magnitude of the discontinuities in heat capacities, Δc_{p1} and Δc_{p2}, are directly correlated to the fraction of each phase, we can look at how composition affects phase fraction. Figure 1.13 is reproduced in Chapter 6 where the two T_g story is thoroughly presented, but is necessary to illustrate this concept. A linear relationship was found between Zr concentration in the alloy and the fraction of phase 1 = $\Delta c_{p1}/(\Delta c_{p1} + \Delta c_{p2})$. The linear relationship of these variables viewed in the context of a rule of mixtures analysis predicts a metastable miscibility gap in the SCLR. This is similar to the phenomenon seen in the phase separating Vitreloy glasses studied by Johnson et al. [15-17] described in Section 1.2, but no annealing is required to cause phase separation. Using a fit to the Zr concentration vs $\Delta c_{p1}/(\Delta c_{p1} + \Delta c_{p2})$ data presented in Chapter 6, we can predict the compositions that should show all phase 1 or all phase 2 by setting $\Delta c_{p1}/(\Delta c_{p1} + \Delta c_{p2}) = 1$ or 0 respectively. Amorphous samples of these compositions showed only single discontinuities in heat capacity as expected from single phase glasses. If this two phase analysis is correct, the endpoints of the miscibility gap have been discovered and the phases into which the alloy separates are known.

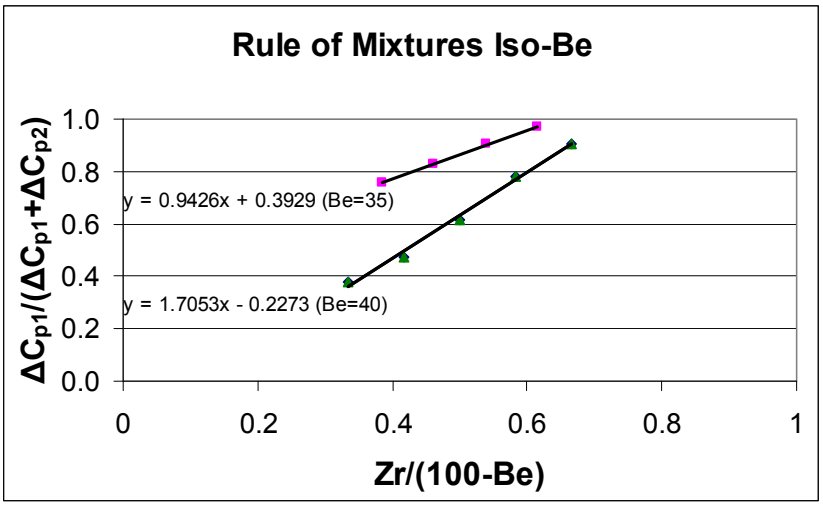

Figure 1.13: Plot of $\Delta c_{p1}/(\Delta c_{p1} + \Delta c_{p2})$ versus Zr concentration gives fraction of phase 1 assuming two glassy phases with similar fragilities. Linear fits indicate rule of mixtures analysis is appropriate and suggests a metastable miscibility gap in SCLR.

The alloy calculated to contain only phase 1 was $Zr_{43}Ti_{17}Be_{40}$. The alloy calculated to contain only phase 2 was $Zr_8Ti_{52}Be_{40}$. If phase separation into these single phase compositions existed in the two T_g alloys, Z contrast imaging in the SEM seemed like a good way to prove their existence. SEM failed to observe the phases suggesting that perhaps the scale of phase separation was too small. This was plausible because Johnson et al. calculated the scale of phase separation was 13nm in Vitreloy compositions from SANS data [15]. TEM work also failed to reveal the two phases. Bright field (BF) and dark field (DF) images showed no evidence of phase separation at nm length scales. Diffraction patterns may have had broadening of the amorphous halo, but were not distinct enough to prove phase separation. Composition analysis was also inconclusive. If the phase separation is very small, on the order of 3 - 5nm or the size of an STZ, the electron interactions with multiple phase regions would be averaged over the thickness of the sample and would mask BF or DF contrast.

It is disheartening not to have microscopic evidence of the two phases. Ternary samples had limited GFA so preparation of a sample for SANS is difficult. SAXS is a good technique for observing composition fluctuations that we are pursuing at Argonne National Labs. We discovered that these samples could be doped with up to 2% Fe without diminishing the apparent two T_g effect and hoped that Mössbauer spectroscopy might reveal two local environments. We doped the two endpoint compositions expected to contain only one phase with 2% Fe and observed two distinct spectra. Two intermediate compositions showing the two T_g phenomenon were also doped with 2% Fe. The two intermediate compositions had Mössbauer spectra identical to the $Zr_8Ti_{52}Be_{40}$ alloy. Various annealing times and temperatures were tried on the two T_g alloys with no

change in the spectra. If we had microscopic evidence of the two phases, we could argue that all the Fe went to the Ti rich phase and therefore all spectra looked like the $Zr_8Ti_{52}Be_{40}$ alloy except the $Zr_{43}Ti_{17}Be_{40}$ composition where the Fe was forced into the Zr rich phase because there was no Ti rich phase present. This explanation seems implausible given the entropic driving force to dissolve impurities in a phase. Additionally there seems to be no insolubility of Fe in the FeZr phase diagram.

The anomalous flow behavior of alloys with an apparent two T_g event was observed and the steeper slope of $\eta(T)$ in the "liquid + liquid" region 3 may be the reason for the higher than expected fragility calculated for $Zr_{35}Ti_{30}Be_{27.5}Cu_{7.5}$ reported in Chapter 4. Chapter 6 clearly shows the presence of two relaxation phenomena in the SCLR of these alloys, but fails to convincingly establish the presence of two phases.

1.6.1 Biocompatible Beryllium???

Appendices A1, A2, and A3 were a digression from the thermodynamics, flow properties and TPF theme of this work, but represent efforts to commercialize a few of the more amazing alloys and led to some important discoveries.

ZrTiBe alloys have high strength, high hardness, good wear characteristics, high corrosion resistance, high elastic limit, and low Young's modulus [57-59]. They fail catastrophically in tension and can show some compressive plasticity in compression [57, 60]. They are less dense than steel, more dense than Al and some compositions approach the density of Ti [57]. The fatigue properties were wonderful according to some groups in 2005 and terrible according to other groups [61-62]. One promising application we saw for these alloys was as orthopaedic hardware.

Hip replacements have some characteristic failure mechanisms. Wear debris can be created as the ball and socket material rub together [63]. This wear debris migrates into the surrounding tissue and causes inflammation. The hardness and good wear characteristics of ZrTiBe glasses could diminish the likelihood of this failure mechanism. Another problem is called stress shielding [64]. The commonly used implant materials have stiffnesses or Young's modulii much higher than bone. As a result, the load on the hip is carried mainly by the metallic implant material and not the bone surrounding it. As a result of this stress shielding, the body decreases the unused bone's density, the implant loosens, and fracture can result. The Young's modulus of ZrTiBe BMG is much lower than the commonly used implant materials and could diminish stress shielding. Another failure mechanism is fatigue cracking [65]. The size and type of artificial hip is determined prior to surgery. If a person gains weight and stresses the hip more than was estimated, fatigue conditions accelerate and the socket joint can fail catastrophically. The good corrosion resistance and high strength of ZrTiBe glasses along with some of the promising fatigue data made us hopeful that the newly discovered alloys would be unaffected by this failure mechanism as well.

The newly invented alloys showed promise to solve some of the mechanical failure mechanisms of hip joints or more broadly orthopaedic hardware, but biocompatibility of these alloys was unknown. Zr and Ti are well known for their biocompatibility. Many alloys free of Ni and Cu had been invented and Ni and Cu are known for poor biocompatibility. Beryllium is a known respiratory toxin, but very little data on cytotoxicity of Be containing alloys was found in the literature. A good indicator of biocompatibility is corrosion resistance [66]. Zr based BMG compositions are known

to have good corrosion resistances in saline environments [67] and biologically relevant solutions [68] and this suggested they might show good biocompatibility.

With limited equipment to test corrosion at Caltech, we chose four highly corrosive solutions, (37% w/w HCl, 0.6M NaCl, 50% w/w NaOH, and 10x phosphate buffered saline (PBS)), to test the corrosion resistance of three metallic glass compositions, ($Zr_{35}Ti_{30}Be_{35}$, $Zr_{35}Ti_{30}Be_{29}Co_6$, and $Zr_{44}Ti_{11}Cu_{10}Ni_{10}Be_{25}$), and three commonly used alloys for biomedical applications (Ti-6Al-4V, 316L Stainless Steel, and CoCrMo). Mass loss measurements were conducted at 1 week, 1 month, and 3 months. Inductively coupled plasma mass spectrometry (ICPMS) measurements were used to analyze the solution for dissolved elements. Details of this study are included in Appendix A1. It was determined from mass loss data that all alloys had excellent corrosion resistance in all solutions except for HCl. ICPMS data was inconclusive for some of the solutions because the amount of dissolved material was below the detection limit.

Corrosion rates in HCl were enormous for most of the alloys tested. $Zr_{44}Ti_{11}Cu_{10}Ni_{10}Be_{25}$ dissolved in under 10 minutes. Most of the other alloys were completely dissolved in 1 week, $Zr_{35}Ti_{30}Be_{35}$ survived for almost 1 month, and the only alloy to survive the full 3 months was CoCrMo which lost 12% of its mass. Corrosion rates in HCl were seen to vary by many orders of magnitude depending on composition. We sought to find the most corrosion resistant BMG for biological applications and given that this was an acidic chloride containing environment, we saw an opportunity to quickly differentiate corrosion resistances in a possibly biologically relevant accelerated corrosion environment.

$Zr_{35}Ti_{30}Be_{35}$ quaternary variants showed the most promise for injection molding so the bulk of the corrosion testing focused on those compositions. Depending on the fourth alloying element, the corrosion rate varied from 10^7 MPY to 50 MPY where MPY is a corrosion penetration rate that measures .001 in / year thickness loss. A plot of standard hydrogen electrode (SHE) half cell potential of the fourth alloying element vs Log(MPY) gave a fairly linear relationship. This was unexpected and has not been satisfactorily explained. The most noble alloying element Pd, when substituted for 4% Be, caused the highest corrosion rate while Al, which has the most anodic half cell potential, when substituted for 5% Be, caused the lowest corrosion rate of the ZrTiBe compositions tested in HCl. The problem with Al addition was that it raised T_g and decreased GFA and ΔT (see Chapter 3). More details can be found in Appendix A1.

$Zr_{35}Ti_{30}Be_{35}$ and $Zr_{35}Ti_{30}Be_{29}Co_6$ were chosen for further biocompatibility testing. $Zr_{35}Ti_{30}Be_{35}$ exhibited one of the best corrosion resistances in HCl, had moderate GFA = 6mm, had a moderate ΔT = 120 °C and good strength to weight ratio. $Zr_{35}Ti_{30}Be_{29}Co_6$ had good corrosion resistance, but much better GFA = 15mm, ΔT = 155 °C, and showed good potential for TPF. Samples were sent to a testing company NAMSA and short term *in vitro* and *in vivo* studies were done to assess biocompatibility. Both alloys performed as well as the control specimen and were considered biocompatible in these short term trials. I took a semester long cell culture class at PCC and had the opportunity to test the cytotoxicity of the 10x PBS solutions in which the metals were tested for corrosion resistance. The solution was diluted to regular 1x strength and no visible damage to the cells resulted after they were exposed to the media and allowed to reach 90% confluence. We became aware of extensive biocompatibility testing performed for Liquidmetal

Technologies on samples of Vitreloy 1 and a glassy composite material called LM2 in an effort to obtain FDA approval. The testing showed that both Vitreloy and the Be containing LM2 were viable as biomaterials and had even passed 1 year *in vivo* studies in New Zealand White Rabbits. The results of the biocompatibility testing are more thoroughly discussed in Appendix A2.

Discussions with Liquidmetal Technologies revealed that the FDA approval process had been abandoned temporarily not because of biocompatibility issues, but because of corrosion fatigue issues with these alloys. Given our improvements in ZrTiBe alloy corrosion resistance we arranged a collaboration with Dr. Liaw at the University of Tennessee, Knoxville and provided $Zr_{35}Ti_{30}Be_{35}$ and $Zr_{35}Ti_{30}Be_{29}Co_6$ samples for corrosion testing in NaCl solutions and corrosion fatigue testing. Our newly invented alloys showed more than an order of magnitude increase in corrosion resistance in simulated sea water solutions as compared to other ZrTi based BMG compositions and even better than other crystalline alloys commonly used in marine environments. Corrosion fatigue results however, were unimproved over other ZrTi based glass forming compositions.

X-ray photoelectron spectroscopy, XPS, studies of the surface chemistry of these new compositions revealed a fully oxidized surface that likely acts as an effective corrosion barrier in static corrosion testing. This oxide layer is expected to have low fracture toughness if the fracture toughnesses of Zr, Ti, or Be oxides are representative of the alloy's surface oxide fracture toughness. As a result of the applied stresses in corrosion fatigue testing, the surface layer cracks allowing the corrosive solution access

to the unoxidized inner material, resulting in a corrosion couple between the inner material and cracked surface layer. More details of this study are found in Appendix A3.

1.7 Introduction Summary

The thermoplastic formability (TPF) of metallic glasses was found to be related to the calorimetrically measured crystallization temperature minus the glass transition temperature, $T_g - T_x = \Delta T$. Alloy development in the ZrTiBe system identified a composition with $\Delta T = 120$ °C. Many alloys with $\Delta T > 150$ °C and one alloy, $Zr_{35}Ti_{30}Be_{27.5}Cu_{7.5}$, with $\Delta T = 165$ °C were discovered by substituting Be with small amounts of fourth alloying elements. The viscosity as a function of temperature, $\eta(T)$, and time temperature transformation (TTT) measurements for the new alloy are presented and combined to create ηTT plots (viscosity time transformation) that are useful in determining what viscosities are available for a required processing time. ηTT plots are created for many alloys used in TPF in the literature and it is found that for processes requiring 60 - 300 s, $Zr_{35}Ti_{30}Be_{27.5}Cu_{7.5}$ provides an order of magnitude lower viscosity for processing than the other metallic glasses. Injection molding is demonstrated with $Zr_{35}Ti_{30}Be_{27.5}Cu_{7.5}$ and the part shows improved mechanical properties over die cast specimens of the same geometry. Changes of slope in $\eta(T)$ measurements were observed and investigated in some quaternary compositions and found to be present in ternary compositions as well. Traditionally metallic glasses show a single discontinuity in heat capacity at the glass transition temperature. Alloys with the changes in slope of $\eta(T)$ were found to show two discontinuities in heat capacity with the changes in slope of $\eta(T)$ roughly correlating with the observed T_g values. These two T_g values were assumed to arise from two glassy phases present in the alloy. Further heat capacity analysis found

systematic trends in the magnitude of the heat capacity discontinuities with composition and the single phase compositions of a metastable miscibility gap were discovered. Microscopic evidence of the two phases is lacking so we must limit our claims to evidence of two relaxation phenomena existing and can't definitively claim two phases.

The alloy development led to the discovery of alloys with densities near Ti that are among the highest strength to weight ratio materials known. Alloys with corrosion resistances in simulated sea water 10x greater than other Zr based glasses and commonly used marine metals were discovered. Glasses spanning 6 orders of magnitude in corrosion resistance to 37% w/w HCl were discovered. Corrosion fatigue in saline environments remains a problem for these compositions and prevents their utility as biomaterials despite good evidence of biocompatibility in *in vitro* and *in vivo* studies.

Chapter 1 References

[1] J. Schroers, W.L. Johnson, R. Busch, Appl. Phys. Lett. 77 (2000) 1158.
[2] S.R. Elliott, Physics of Amorphous Materials, second ed., John Wiley & Sons Inc., New York, 1990, pp. 29-69.
[3] J. Schroers, A. Masuhr, W.L. Johnson, R. Busch, Phys. Rev. B 60 (1999) 11855.
[4] A. Peker, W.L. Johnson, Appl. Phys. Lett. 63 (1993) 2342.
[5] Y.J. Kim, R. Busch, W.L. Johnson, A.J. Rulison, W.K. Rhim, Appl. Phys. Lett. 68 (1996) 1057.
[6] H. Vogel, Z. Phys. 22 (1921) 645.
[7] W.L. Johnson, M.D. Demetriou, J.S. Harmon, M.L. Lind, K. Samwer, MRS Bull. 32 (2007) 644.
[8] M.C. Lee, J.M. Kendall, W.L. Johnson, Appl. Phys. Lett. 40 (1982) 382.
[9] W.L. Johnson, Amorphe Metallische Werkstoffe 14, Metalltagung in der DDR (1981) 183.
[10] R. Schulz, K. Samwer, W.L. Johnson, J. Non-Cryst. Solids 61 & 62 (1984) 997.
[11] L.E. Tanner, R. Ray, Scripta Metal. 11 (1977) 783.
[12] R. Hasegawa, L.E. Tanner, Phys. Rev. B 16 (1977) 3925.
[13] L.E. Tanner, R. Ray, Acta Metall. 27 (1979) 1727.
[14] L.E. Tanner, R. Ray, Scripta Metall. 14 (1980) 657.
[15] S. Schneider, P. Thiyagarajan, U. Geyer, W.L. Johnson, MRS Technical Report DOI 10.2172/510428 (1996).
[16] S. Schneider, P. Thiyagarajan, U. Geyer, W.L. Johnson, Physica B 241 (1998) 918.

[17] S. Schneider, U. Geyer, P. Thiyagarajan, W.L. Johnson, Materials Science Forum Vols. 235-238 (1997) 337.
[18] W. Liu, W.L. Johnson, S. Schneider, U. Geyer, P. Thiyagarajan, Phys. Rev. B 59 (1999) 11755.
[19] Q. Zhang, W. Zhang, G. Xie, A. Inoue, Mater. Sci. Eng. B 148 (2008) 97.
[20] B.J. Park, H.J. Chang, D.H. Kim, W.T. Kim, K. Chattopadhyay, T.A. Abinandanan, S. Bhattacharyya, Phys. Rev. Lett. 96 (2006) 245503.
[21] R.G. Hennig, A.E. Carlsson, K.F. Kelton, C.L. Henley, Phys. Rev. B 71 (2005) 144103.
[22] X.P. Tang, J.F. Löffler, W.L. Johnson, Y. Wu, J. Non-Cryst. Solids 317 (2003) 118.
[23] B. Van de Moortele, T. Epicier, J.L. Soubeyroux, J.M. Pelletier, Phil. Mag. Lett. 84 (2004) 245.
[24] G. Wang, J. Shen, J.F. Sun, B.D. Zhou, J.D. Fitz Gerald, D.J. Llewellyn, Z.H. Stachurski, Scripta Mater. 53 (2005) 641.
[25] J.H. Na, Y.C. Kim, W.T. Kim, D.H. Kim, Met. Mater. Int. 14 (2008) 553.
[26] G. Kumar, D. Nagahama, M. Ohnuma, T. Ohkubo, K. Hono, Scripta Mater. 54 (2006) 801.
[27] D. Nagahama, T. Ohkubo, K. Hono, Scripta Mater. 49 (2003) 729.
[28] T. Abe, M. Shimono, K. Hashimoto, K. Hono, H. Onodera, Scripta Mater. 55 (2006) 421.
[29] J. Schroers, Acta Mater. 56 (2008) 471.
[30] J. Schroers, JOM 57 (2005) 35.
[31] J. Schroers, N. Paton, Adv. Mater. Processes 164 (2006) 61.
[32] T. Masumoto, A. Inoue, N. Nishiyama, H. Horimura, T. Shibata, US Patent #6027586.
[33] T. Masumoto, A. Inoue, J. Nagahora, K. Kita, US Patent #5209791.
[34] K.S. Lee, Y.W. Chang, Mater. Sci. Eng. A 399 (2005) 238.
[35] Y. Saotome, K. Imai, S. Shioda, S. Shimizu, T. Zhang, A. Inoue, Intermetallics 10 (2002) 1241.
[36] J. Schroers, Q. Pham, A. Peker, N. Paton, R.V. Curtis, Scripta Mater. 57 (2007) 341.
[37] G. Duan, A. Wiest, M.L. Lind, J. Li, W.K. Rhim, W.L. Johnson, Adv. Mater. 19 (2007) 4272.
[38] Y. Li, S.J. Poon, G.J. Shiflet, J. Xu, D.H. Kim, J.F. Löffler, MRS Bull. 32 (2007) 624.
[39] A.L. Greer, E. Ma, MRS Bull. 32 (2007) 611.
[40] B.A. Legg, J. Schroers, R. Busch, Acta Mater. 55 (2007) 1109.
[41] T. Waniuk, J. Schroers, W.L. Johnson, Phys. Rev. B 67 (2003) 184203.
[42] J. Schroers, W.L. Johnson, Appl. Phys. Lett. 84 (2004) 3666.
[43] G.J. Fan, H.J. Fecht, E.J. Lavernia, Appl. Phys. Lett. 84 (2004) 487.
[44] J.P. Chu, H. Wijaya, C.W. Wu, T.R. Tsai, C.S. Wei, T.G. Nieh, J. Wadsworth, Appl. Phys. Lett. 90 (2007), 034101.
[45] A. Masuhr, T.A. Waniuk, R. Busch, W.L. Johnson, Phys. Rev. Lett. 82 (1999) 2290.
[46] R. Busch,W.L. Johnson, Appl. Phys. Lett. 72 (1998) 2695.

[47] F. Spaepen, Acta Metall. 25 (1977) 407.
[48] J. Lu, G. Ravichandran,W.L. Johnson, Acta Mater. 21 (2003) 3429.
[49] L. Kaufman, L.E. Tanner, CALPHAD 3 (1979) 91.
[50] L.E. Tanner, R. Ray, C.F. Cline, US Patent #3989517.
[51] L.E. Tanner, R. Ray, C.F. Cline, US Patent #4050931.
[52] A. Peker, W.L. Johnson, US Patent #5288344.
[53] G. Duan, A. Wiest, W.L. Johnson, US Patent Application #20080121316.
[54] G. Duan, A. Wiest, M.L. Lind, A. Kahl, W.L. Johnson, Appl. Phys. Lett. 90 (2007) 211901.
[55] M.D. Demetriou, A. Wiest, W.L. Johnson, US Patent Application #20090162629.
[56] J.F. Löffler, J. Schroers, W.L. Johnson, Appl. Phys. Lett. 77 (2000) 681.
[57] G. Duan, A. Wiest, M.L. Lind, A. Kahl, W.L. Johnson, Scripta Mater. 58 (2008) 465.
[58] A. Wiest, G.Y. Wang, L. Huang, S. Roberts, M.D. Demetriou, P.K. Liaw, W.L. Johnson, Scripta Mater. in review.
[59] M.Z. Ma, R.P. Liu, Y. Xiao, D.C. Lou, L. Liu, Q. Wang, W.K. Wang, Mater. Sci. Eng. A 386 (2004) 326.
[60] D.C. Hofmann, J.Y. Suh, A. Wiest, G. Duan, M.L. Lind, M.D. Demetriou, W.L. Johnson, Nature 451 (2008) 1085.
[61] G.Y. Wang, P.K. Liaw, A. Peker, B. Yang, M.L. Benson, W. Yuan, W.H. Peter, L. Huang, M. Freels, R.A. Buchanan, C.T. Liu, C.R. Brooks, Intermetallics 13 (2005) 429.
[62] C.J. Gilbert, J.M. Lippmann, R.O. Ritchie, Scripta Mater. 38 (1998) 537.
[63] C.R. McMillin, in: B.D. Ratner, A.S. Hoffman, F.J. Schoen, J.E. Lemons (Eds.), Biomaterials Science: An Introduction to Materials in Medicine, Academic Press, California, 1996, pp. 267-271.
[64] J. Black, Biological Performance of Materials: Fundamentals of biocompatibility, fourth ed., CRC Press, Florida, 2006.
[65] M. Niinomi, T. Hattori, T. Kasuga, H. Fukui, in: G.E. Wnek, G.L. Bowlin (Eds.), Encyclopedia of Biomaterials and Biomedical Engineering, second ed., Informa Healthcare USA, Inc., New York, 2008, pp. 2876-2892.
[66] G.L. Burke, Can. Med. Assoc. J. (1940) 125.
[67] M.L. Morrison, R.A. Buchanan, P.K. Liaw, B.A. Green, G.Y. Wang, C.T. Liu, J.A. Horton, Mater. Sci. Eng. A 467 (2007) 198.
[68] M.L. Morrison, R.A. Buchanan, R.V. Leon, C.T. Liu, B.A. Green, P.K. Liaw, J.A. Horton, J. Biomed. Mater. Res. Part A 74 (2005) 430.